Combustion of thermally thick wood particles: A study on the influence of wood particle size on the combustion behavior

Inge Haberle,*,† Nils Erland L. Haugen,†,‡ and Øyvind Skreiberg‡

Department of Energy and Process Engineering, Norwegian University of Science and Technology, Kolbjørn Hejes vei 1 B, 7491 Trondheim, Norway, and Department of Thermal Energy, SINTEF Energy Research, Kolbjørn Hejes vei 1 A, 7491 Trondheim, Norway

E-mail: inge.haberle@ntnu.no

Phone: +47 73 593697. Fax: -

[1]

*To whom correspondence should be addressed

†Norwegian University of Science and Technology

‡SINTEF Energy Research

This is the accepted version of an article published in Energy and Fuels
DOI: 10.1021/acs.energyfuels.8b00777

Abstract

A one-dimensional (1D) comprehensive combustion model for thermally thick wet wood particles, which is also applicable for studying large wood logs, is developed. The model describes drying, devolatilization and char gasification as well as char oxidation. Furthermore, CO oxidation is modeled, in order to account for the fact that exiting gas products can be oxidized and therefore limit the oxygen transportation to the active sites. The challenges for model validation are outlined. Model validation was done against experimental data for combustion of near-spherical wood particles. Furthermore, the validated model was up-scaled and the effect of wood log diameter on the thermal conversion time, the extent as well as the position of drying, devolatilization and char conversion zones were studied. The upscaling was done for cylindrical wood logs with an aspect ratio of 4. The thermal conversion time significantly increased with the size. It was also found that the relative extent of the drying, devolatilization and char conversion zones decreased as wood log size increased. The paper concludes with recommendations for future works.

This is the accepted version of an article published in Energy and Fuels
DOI: 10.1021/acs.energyfuels.8b00777

Contents

This is the accepted version of an article published in Energy and Fuels
DOI: 10.1021/acs.energyfuels.8b00777

1 Introduction

Wood has caught the attention of numerous researchers due to its important role as a renewable energy source. Its applications are broad with an enhanced usage within the field of thermal conversion, where a wide range of particle sizes is used.[1] Over the last decades the designs of the combustion units used to thermochemically convert wood, e.g. wood stoves, were improved based on experimental studies. However, a more cost-efficient optimization route is the combination of modeling and experiments.[2] Therefore it is of interest to focus on model development describing thermochemical conversion of wood. However, if a wood combustion model shall be embedded in a simulation tool that is used for design and optimization purposes of wood combustion units, an accurate description of the char conversion stage, in addition to the implementation of detailed drying and devolatilization models, is crucial. The reason why char conversion is considered a key part of an accurate solid phase model is that the char conversion stage is significantly slower than drying and devolatilization and hereby influences the total thermal conversion time. Consequently, the char burnout time has a significant effect on the design of a combustion unit. In addition, a significant amount of the thermal energy is stored in the char.

There is already a number of combustion models available.[1,3–11] Two different modeling concepts are used: the layer (or interface) approach[3,4,7,9–11] and the mesh-based approach.[1,5,6,8] A more detailed analysis of currently available thermal wood conversion models is presented by Haberle et al.[12] Still, compared to modeling work related to thermal coal conversion, the literature on wood particles is limited.

Even though numerous studies on coal combustion are available in the open literature these studies are not directly relevant for wood combustion modeling since wood and coal are very different fuels, with wood having a higher volatile content and a lower energy density.[13] The volatile content in biomass is around 80 % compared to only around 30% for coal.[14] In addition, while the pore structure of coal is isotropic, the pore structure of biomass is *non*-isotropic.

This is the accepted version of an article published in Energy and Fuels
DOI: 10.1021/acs.energyfuels.8b00777

Due to the significantly higher volatile content of biomass, biomass has a longer devolatilization stage compared to coal. In fact these two fuels differ significantly in ignition temperature, ignition delay and burnout times. For biomass conversion, volatiles can more easily exit the particle through its porous structure. In coal particles on the other hand, the internal pressure increases more, due to its lower porosity and if the pressure becomes high enough, the walls in the particle break while suddenly releasing the volatiles in jets.[15] This different behavior in volatile release affects the volatiles combustion time. While the combustion time of volatile matter of biomass takes 40 - 50 % of the total combustion time, it only takes 10 - 20 % of the total combustion time of coal particles.[15] All these aspects highlight that wood combustion models are not simply compatible with coal combustion models and wood combustion models therefore have to be considered as an independent area of research where further development is needed.

Yang et al.[1] studied the combustion characteristics of biomass, with a special focus on the particle size range from 10 μm to 20 mm. This was done both experimentally and with a two-dimensional (2D) mesh-based model. Their char conversion model does not explicitly consider the diffusion of oxygen to the active sites, and also only considers oxidation reactions, while fully neglecting both steam and CO_2 gasification.[1] However, it has been reported by other researchers that in the case of significantly wet particles being thermally converted, the available water vapor leaving the inner parts of the particle where drying and devolatilization still occur, passes through the hot char zones, where it can act as gasifying agent.[16] Yang et al.[1] used a simplified one-step global devolatilization model, which requires a pre-defined ratio between produced char and gases. This means that the char content does not automatically change depending on the heating rate. This behavior can be accurately predicted with more advanced devolatilization models, e.g. with three independent competitive reactions. Yang et al.[1] found that the influence of particle shape on the particle's combustion behavior is crucial. They also found that due to the ignition of the released volatiles, the particle temperature increased. As a consequence, also the volatile

This is the accepted version of an article published in Energy and Fuels
DOI: 10.1021/acs.energyfuels.8b00777

release and the char burning rate were accelerated. This trend was observed for all particle sizes tested. The time until this volatile gas ignition occurred, increased as particle size increased.

Lu et al.[5] developed a one-dimensional (1D) model describing wood combustion and presented experimental data as well as modeling results of combustion characteristics of differently sized particles, within a size range of 3 to 15 mm. Furthermore, they studied different shapes of particles, with their model being able to describe combustion of cylinders, spheres and flat plates. Due to the non-isotropic nature of biomass, it is not clear, however, how well multi-dimensional physics is reproduced by the use of simple bridge factors in a 1D model.

Besides the more obvious influence of particle size and shape on combustion behavior, there is also current research effort on identifying the influence of thermal pre-treatment of wood on its combustion behavior.[17] These studies were performed with spherical particles with a size range of 3 to 5 mm. The combustion behavior of torrefied particles was studied and it was found that for such particles the devolatilization time was linearly dependent on the mass of the tested sample. It was also shown that for raw biomass particles, within the same particle size range, the char burnout time also increased linearly with increasing biomass mass.[17]

The current paper presents a study on how particle size affects the combustion of large thermally thick wood particles and logs by means of a 1D mesh-based model. Therefore the paper first presents the validation of the model. Experimental data was available for a thermally thick, near-spherical particle (aspect ratio of 1), and validation was done for such wood particles. After validation, the model was up-scaled to larger cylindrical wood logs. This was done because the model will be used for simulating the thermochemical degradation and char conversion in typical wood stoves. Here, we define a wood log as a thermally thick wood particle that has a size in the cm-range and typically an aspect ratio larger than 4.

Even though there are works available studying the combustion characteristics of differ-

This is the accepted version of an article published in Energy and Fuels
DOI: 10.1021/acs.energyfuels.8b00777

ently sized wood particles, none of those works focused on wood particles of sizes close to wood logs used for combustion in wood stoves. The influence of particle size is expected to be very important when modeling thermal biomass conversion, as it involves a closely coupled interaction between chemistry and heat and mass transfer processes with emphasis on the fact that the mentioned transfer phenomena are affected by particle size.[1] Furthermore, the paper also includes a detailed discussion on grid-independence and the requirements for the 1D-mesh to obtain a grid-independent solution. In addition, the challenges for model validation of a thermal conversion model, with focus on char conversion modeling validation are discussed.

Finally, it should be noted that for highly detailed simulation models, like the ones being used here, a number of input data are required in order for the simulation tool to yield reliable results. These input data, such as permeability, internal surface area or thermal conductivity, are typically determined for different wood species in specially designed experiments. As part of the model development and validation we therefore also aimed for testing and running the model with the best available key input data that can be found in current literature

2 Numerical modeling

A 1D mesh-based model for drying, devolatilization and char conversion of a wet thermally thick cylindrical wood particles was developed. The differentiation between particle and log was done, based on the shape that was tested. Near-spherical particles were considered as particles, while wood particles with an aspect ratio larger than 1, and consequently considered cylindrical, were referred to as wood logs in this work.

Mesh-based models are comprehensive models, that divide the particle into a large number of shells (in case of a cylindrical or spherical particle). At every grid point, solid, liquid and gas phases are present and the gas phase consist of a number of gas species. The model includes the evolution equations for wood density, char density, ash density, total gas phase,

This is the accepted version of an article published in Energy and Fuels
DOI: 10.1021/acs.energyfuels.8b00777

gas phase species, temperature and liquid free water as well as bound water. The water content exceeding the fiber saturation point (for most wood species 30wt%, dry basis) is classified as liquid free water, while the water content below the fiber saturation point is classified as bound water. The convective and diffusive transport of the gas phase within the porous structure is modeled. Furthermore, the liquid phase can be transported by diffusion (if defined as bound water) or by convection (if defined as liquid free water). However, the transport of liquid free water has been found to be negligible during high temperature drying,[18] and it has therefore been deactivated in the current model. Drying is modeled either by the kinetic rate model or the thermal drying model. Devolatilization is described by a three independent competitive reactions scheme in the primary devolatilization stage and subsequent secondary tar reactions. More details on the scheme can be found in earlier works.[18] In the following sub-section the applied governing equations are discussed in more detail.

2.1 Governing equations

A detailed discussion of the governing equations relevant for drying and devolatilization has been presented in an earlier work by Haberle et al.[18] Nonetheless, the most relevant equations are given in Table 1 and Table 2.

This is the accepted version of an article published in Energy and Fuels
DOI: 10.1021/acs.energyfuels.8b00777

Table 1: List of evolution equations that have to be implemented for the drying and devolatilization model. The last column gives the relevant references.

Evolution equation		**Ref.**
Wood density[1)]	$\frac{\partial \rho_{\mathrm{wood}}}{\partial t} = -(k_1 + k_2 + k_3)\rho_{\mathrm{wood}} - \frac{\rho_{\mathrm{wood}}}{V_j}\frac{\partial V_j}{\partial t}$	19
Ash density	$\frac{\partial \rho_{\mathrm{ash}}}{\partial t} = -\frac{\rho_{\mathrm{ash}}}{V_j}\frac{\partial V_j}{\partial t}$	5
Gas phase continuity equation	$\frac{\partial \epsilon_{\mathrm{g}} \rho_{\mathrm{g}}^{\mathrm{g}}}{\partial t} + \frac{1}{r}\frac{\partial (r \epsilon_{\mathrm{g}} \rho_{\mathrm{g}}^{\mathrm{g}} u_{\mathrm{r}})}{\partial r} = \dot{\omega}_{\mathrm{g}}$	5
Species mass fraction	$\frac{\partial (\epsilon_{\mathrm{g}} \rho_{\mathrm{g}}^{\mathrm{g}} Y_k)}{\partial t} + \frac{1}{r}\frac{\partial (r \epsilon_{\mathrm{g}} \rho_{\mathrm{g}}^{\mathrm{g}} Y_{\mathrm{k}} u_{\mathrm{r}})}{\partial r} = \frac{1}{r}\frac{\partial}{\partial r}\left(r \epsilon_{\mathrm{g}} \rho_{\mathrm{g}}^{\mathrm{g}} D_{\mathrm{eff}} \frac{\partial Y_{\mathrm{k}}}{\partial r} \right) + \dot{\omega}_k$	5
Char density[2)]	$\frac{\partial \rho_{\mathrm{char}}}{\partial t} = k_3 \rho_{\mathrm{wood}} + \epsilon_{\mathrm{g}} k_5 \rho_{\mathrm{tar}}^{\mathrm{g}} - \frac{\rho_{\mathrm{char}}}{V_j}\frac{\partial V_j}{\partial t}$	19
Temperature	$\left(\rho_{\mathrm{wood}} c_{P,\mathrm{wood}} + \rho_{\mathrm{char}} c_{P,\mathrm{char}} + \rho_{\mathrm{l}} c_{P,\mathrm{l}} + \rho_{\mathrm{b}} c_{P,\mathrm{b}} + \epsilon_{\mathrm{g}} \rho_{\mathrm{g}}^{\mathrm{g}} c_{P,\mathrm{g}} \right) \frac{\partial T}{\partial t} + \left(\rho_{\mathrm{l}} c_{\mathrm{P,l}} u_{\mathrm{l}} + \rho_{\mathrm{b}} c_{\mathrm{P,b}} u_{\mathrm{b}} + \epsilon_{\mathrm{g}} \rho_{\mathrm{g}}^{\mathrm{g}} c_{\mathrm{P,g}} u_{\mathrm{r}} \right) \frac{\partial T}{\partial r} = \frac{1}{r}\frac{\partial}{\partial r}\left(r \lambda_{\mathrm{eff}} \left(\frac{\partial T}{\partial r} \right) \right) - \Phi_{\mathrm{evap}} - \Phi_{\mathrm{devol,1}} + \Phi_{\mathrm{devol,2}}$	20
Liquid free water	$\frac{\partial \rho_{\mathrm{l}}}{\partial t} + \frac{1}{r}\frac{\partial (r \rho_{\mathrm{l}} u_{\mathrm{l}})}{\partial r} = -\dot{\omega}_{\mathrm{evap,l}}$	21
Bound water	$\frac{\partial \rho_{\mathrm{b}}}{\partial t} = \frac{1}{r}\frac{\partial}{\partial r}\left(r D_{\mathrm{b}} \frac{\partial \rho_{\mathrm{b}}}{\partial r} \right) - \dot{\omega}_{\mathrm{evap,b}}$ [3)]	21

[1)] The reaction rates of wood to non-condensable gases, tar and char are given by k_1, k_2 and k_3, respectively.
[2)] k_5 marks the reaction of tar to char.
[3)] obtained under assumption of constant wood density until drying is accomplished.

This is the accepted version of an article published in Energy and Fuels
DOI: 10.1021/acs.energyfuels.8b00777

Table 2: List of additional equations that are required for a drying and devolatilization model. The last column gives the relevant references.

Additional equation		**Ref.**
Radial gas phase velocity	$u_{\mathrm{r}} = -\frac{\kappa}{\mu_{\mathrm{g}}}\frac{\partial P_{\mathrm{g}}}{\partial r}$	5
Ideal equation of state	$P_{\mathrm{g}} = \frac{\rho_{\mathrm{g}}^{\mathrm{g}} RT}{MW_{\mathrm{mix,total}}}$	5
Reaction rates of devolatilization	$k_i = A_i \exp\left(\frac{-E_{\mathrm{a,i}}}{RT}\right)$	5
Liquid free water velocity	$u_{\mathrm{l}} = -\frac{\kappa_{\mathrm{l}}}{\mu_{\mathrm{l}}}\frac{\partial P_{\mathrm{l}}}{\partial r}$	21
Liquid pressure[1)]	$P_{\mathrm{l}} = P_{\mathrm{g}} - P_{\mathrm{c}}$	21
Fraction of residual wood	$\eta = \frac{\rho_{\mathrm{wood}}}{\rho_{\mathrm{wood,0}}}$	
Effective thermal conductivity[5)]	$\lambda_{\mathrm{eff}} = \epsilon_{\mathrm{pore}}(1-\phi)\lambda_{\mathrm{g}} + \epsilon_{\mathrm{pore}}\phi\lambda_{\mathrm{l}}$ $+(1-\epsilon_{\mathrm{pore}})\Big(\lambda_{\mathrm{wood}}\frac{\rho_{\mathrm{wood}}}{\rho_{\mathrm{wood}}+\rho_{\mathrm{char}}+\rho_{\mathrm{ash}}}$ $+\lambda_{\mathrm{char}}\frac{\rho_{\mathrm{char}}}{\rho_{\mathrm{wood}}+\rho_{\mathrm{char}}+\rho_{\mathrm{ash}}} + \lambda_{\mathrm{ash}}\frac{\rho_{\mathrm{ash}}}{\rho_{\mathrm{wood}}+\rho_{\mathrm{char}}+\rho_{\mathrm{ash}}}\Big)$ $+\frac{\epsilon_{\mathrm{g}}\sigma T^3 d_{\mathrm{pore}}}{\omega_{\mathrm{pore}}}$	
Effective permeability[2)]	$\kappa_{\mathrm{eff}} = \xi(\eta\kappa_{\parallel,\mathrm{wood}} + (1-\eta)\kappa_{\parallel,\mathrm{char}})$ $+(1-\xi)(\eta\kappa_{\perp,\mathrm{wood}} + (1-\eta)\kappa_{\perp,\mathrm{char}})$	
Bound water diffusivity	$D_{\mathrm{b}} = 7\times10^{-6}\exp\left(\frac{-4633+3523\frac{\rho_{\mathrm{b}}}{\rho_{\mathrm{wood}}}}{T}\right)$	21
Knudsen diffusivity, $\mathrm{D_{Knudsen}}$	$D_{\mathrm{Knudsen}} = \frac{2r_{\mathrm{pore}}}{3}\sqrt{\left(8RT/\pi MW_i\right)}$	8
Effective diffusivity, $\mathrm{D_{eff}}$	$D_{\mathrm{eff}} = \left(1/\left(\frac{1}{D_{\mathrm{AB}}} + \frac{1}{D_{\mathrm{Knudsen}}}\right)\right)\epsilon_{\mathrm{pore}}^2$	8
Evaporation bound water	$\dot{\omega}_{\mathrm{evap,b}} = A_{\mathrm{evap}}\exp\left(\frac{-E_{\mathrm{a,evap}}}{RT}\right)\rho_{\mathrm{b}}$	
Evaporation liquid free water[3)]	$\dot{\omega}_{\mathrm{evap,l}} = f_{\mathrm{evap}}\frac{F_{\mathrm{heat}}}{\triangle h_{\mathrm{evap}}}$, with $F_{\mathrm{heat}} = \frac{1}{r}\frac{\partial}{\partial r}\left(r\epsilon_{\mathrm{g}}\rho_{\mathrm{g}}^{\mathrm{g}}u_{\mathrm{r}}c_{\mathrm{P,g}}T - r\lambda_{\mathrm{eff}}\frac{\partial T}{\partial r}\right)$	8
Gas phase volume fraction	$\epsilon_{\mathrm{g}} = \epsilon_{\mathrm{pore}}(1-\phi) = \frac{V_{\mathrm{g}}}{V}$	21
Porosity	$\epsilon_{\mathrm{pore}} = \frac{V_{\mathrm{pore}}}{V}$	21
Phase average liquid free density[4)]	$\rho_{\mathrm{l}} = \rho_{\mathrm{l}}^{\mathrm{l}}\phi\epsilon_{\mathrm{pore}}$	21
Phase average gas phase[4)]	$\rho_{\mathrm{g}} = \rho_{\mathrm{g}}^{\mathrm{g}}(1-\phi)\epsilon_{\mathrm{pore}}$	21

[1)] P_{c} is the capillary pressure, which is commonly described by expressions obtained from experimental observations. In this model we used $P_{\mathrm{c}} = 10000\left(\frac{\rho_{\mathrm{wood,0}}M_{\mathrm{l}}}{\epsilon_{\mathrm{pore}}\rho_{\mathrm{l}}}\right)^{-0.61}$ also used by de Paiva Souza and Nebra.[22]

[2)] ξ is the bridge factor.

[3)] The latent heat of vaporization, $\triangle h_{\mathrm{evap}}$, was 2.44×10^6 J/kg.[5]

[4)] $\rho_{\mathrm{l}}^{\mathrm{l}}$ and $\rho_{\mathrm{g}}^{\mathrm{g}}$ are the intrinsic phase average densities of liquid and gas phase, respectively, while ϕ is the volume fraction of pores filled with liquid free water.

[5)] The effective thermal conductivity for wood and char in the solid phase has been taken from Fatehi and Bai[8] and extended to also include the influence of ash and liquid free water and bound water.

This is the accepted version of an article published in Energy and Fuels
DOI: 10.1021/acs.energyfuels.8b00777

The numerical model describing char conversion includes oxidation of char

$$C + xO_2 \rightarrow aCO + bCO_2 \tag{R1}$$

as well as steam gasification

$$C + H_2O \rightarrow H_2 + CO \tag{R2}$$

and CO_2 gasification

$$C + CO_2 \rightarrow 2CO. \tag{R3}$$

Compared to the pure drying and devolatilization model, the source term in the gas phase continuity equation, $\dot{\omega}_{\mathrm{g}}$, (see Table 1) has to be changed in order to also consider char oxidation and gasification reactions such that

$$\dot{\omega}_{\mathrm{g}} = \dot{\omega}_{\mathrm{k_1,k_2}} - \dot{\omega}_{\mathrm{k_5}} + \dot{\omega}_{\mathrm{evap}} + \dot{\omega}_{\mathrm{oxid}}\Omega_1\frac{MW_{\mathrm{C}}}{MW_{\mathrm{O_2}}} + \dot{\omega}_{\mathrm{H_2O,gasif}}\Omega_2\frac{MW_{\mathrm{C}}}{MW_{\mathrm{H_2O}}} + \dot{\omega}_{\mathrm{CO_2,gasif}}\Omega_3\frac{MW_{\mathrm{C}}}{MW_{\mathrm{CO_2}}} \tag{1}$$

where $\dot{\omega}_{\mathrm{oxid}}$ is the reaction rate due to char oxidation while $\dot{\omega}_{\mathrm{H_2O,gasif}}$ and $\dot{\omega}_{\mathrm{CO_2,gasif}}$ are the reaction rates due to steam and CO_2 gasification, respectively. The first three terms on the right hand side of Eq. (1) are due to primary devolatilization reactions of wood to non-condensable gases and tar, respectively, $\dot{\omega}_{\mathrm{k_1,k_2}}$, secondary tar reactions to char, $\dot{\omega}_{\mathrm{k_5}}$, and evaporation, $\dot{\omega}_{\mathrm{evap}}$, respectively. The stoichiometric coefficients of the different char consumption reactions are given by Ω_2 (=1) and Ω_3 (=1), respectively, corresponding to the coefficients in R2 and R3. Reaction R1 has been taken from Evan and Emmons[23] with the following definitions of coefficients

$$a + b = 1 \tag{2}$$

and

$$x = \frac{a}{2} + b. \tag{3}$$

This is the accepted version of an article published in Energy and Fuels
DOI: 10.1021/acs.energyfuels.8b00777

Their modeling assumption of a temperature-dependent ratio between CO/CO_2 [23]

$$\frac{a}{b} = 4.3 \exp\Big(-3390/T \Big) \tag{4}$$

has been simplified by setting $a = 1$ and therefore neglecting the temperature-dependency. As a consequence $\Omega_1 = 2$ in R1. This simplification was done, since the model developed in this work was partly also compared against previous modeling results by Fatehi and Bai [8] and Lu et al.,[5] both only assuming heterogeneous char reactions to form CO. Despite the fact that a temperature-dependent CO/CO_2 ratio is more accurate, it has not been considered in the current work in order to ease validation against other modeling works.

The primary devolatilization reactions describe the formation of non-condensable gases, k_1, and tar, k_2, from wood, such that

$$\dot{\omega}_{\mathrm{k_1,k_2}} = (k_1 + k_2)\rho_{\mathrm{wood}}. \tag{5}$$

In Eq. (5), ρ_{wood} refers to the apparent wood density. The secondary tar cracking reaction, $\dot{\omega}_{\mathrm{k_5}}$, describe the reaction of tar to char such that

$$\dot{\omega}_{\mathrm{k_5}} = k_5 \rho^{\mathrm{g}}_{\mathrm{tar}} \epsilon_{\mathrm{g}}, \tag{6}$$

where $\rho^{\mathrm{g}}_{\mathrm{tar}}$ is the intrinsic tar density and k_5 is the reaction rate constant of tar to char. The third term on the right hand side of Eq. (1) refers to water vapor formation due to drying, which can be modeled either by the kinetic rate drying model or the thermal drying model (see Table 2). More information on the drying stage can be found in an earlier work by Haberle et al.[18]

Besides the gas phase continuity equation, also char mass evolution and gas phase species equations have to be modified when char conversion is included in the model. The char mass

This is the accepted version of an article published in Energy and Fuels
DOI: 10.1021/acs.energyfuels.8b00777

evolution is described by

$$\frac{\partial \rho_{\text{char}}}{\partial t} = \dot{\omega}_{\text{k}_3} + \dot{\omega}_{\text{k}_5} - \dot{\omega}_{\text{oxid}} \Omega_1 \frac{MW_{\text{C}}}{MW_{\text{O}_2}} - \dot{\omega}_{\text{H}_2\text{O,gasif}} \Omega_2 \frac{MW_{\text{C}}}{MW_{\text{H}_2\text{O}}} - \dot{\omega}_{\text{CO}_2\text{,gasif}} \Omega_3 \frac{MW_{\text{C}}}{MW_{\text{CO}_2}} \tag{7}$$

where

$$\dot{\omega}_{\text{k}_3} = k_3 \rho_{\text{wood}} \tag{8}$$

includes the reactions of wood to char due to primary devolatilization reactions, while k_3 is the corresponding reaction rate constant.

The heterogeneous char conversion reactions describing char conversion can be implemented in the model as[5]

$$\dot{\omega}_{\text{i}} = s_{\text{a,char}} \frac{\rho_{\text{char}}}{\rho_{\text{char}} + \rho_{\text{wood}} + \rho_{\text{ash}}} k_i \epsilon_{\text{g}} \rho_{\text{g}}^{\text{g}} Y_k \tag{9}$$

where the reaction rate constants of reactions R1 to R3, k_i, are described by a temperature-dependent Arrhenius expression such that[5]

$$k_i = A_i T \exp\left(\frac{-E_{\text{a,i}}}{RT}\right), \tag{10}$$

with A_i being the pre-exponential factor, $E_{\text{a,i}}$ the activation energy, R the ideal gas constant and T the temperature. The subscript i, in Eq. (9) and Eq. (10), refers to the different char conversion reactions mentioned in R1 to R3. Furthermore, the term $\frac{\rho_{\text{char}}}{\rho_{\text{char}}+\rho_{\text{wood}}+\rho_{\text{ash}}}$ is included in Eq. (9) to account for the decreasing fraction of surface area occupied by char due to ongoing char conversion. This is a valid assumption, as it has also been shown by Wornat et al.[24] that the reactivity of two different biomass chars was reduced during char conversion. The reason herefore was stated to be an ongoing depletion of more reactive carbon, and the physical and chemical alteration of available inorganic compounds, which caused them to be less catalytically active.[24]

Metal release during biomass combustion was not considered in this work and therefore

This is the accepted version of an article published in Energy and Fuels
DOI: 10.1021/acs.energyfuels.8b00777

also the catalytic effect of potassium was neglected. This is a valid assumption since for large thermally thick wood particles, as those studied here, the conversion is dominated by transport phenomena and not by reaction kinetics.[1]

Spruce has an initial oxygen content of 43.5 % while for birch the value is 44.3 %. Consequently, hardwoods and softwoods both have a high oxygen content, and the resulting chars also still contain oxygen within the range of 5.1 to 6.4 % for birch char and spruce char, respectively.[7] For simplicity, this oxygen content is not considered while modeling char oxidation.

In Eq. (9) the reaction order is set to unity. Char reactivity depends on the solid feedstock as well as the devolatilization conditions, which affect the pore structure of the char and the elemental composition. It has been suggested that the differences in the char reactivity derived from wood species can be taken into consideration by adjusting the pre-exponential factor as well as the reaction order.[25] However, in this work, the reaction order was set to unity, which is a common modeling approach, see e.g. Fatehi and Bai[8] or Lu et al.[5]

One main difference of a comprehensive numerical model including all three stages of thermal conversion and a model that is focusing solely on drying and devolatilization is an increase in the number of considered gas phase species. While a pure drying and devolatilization model does not require an explicit consideration of H_2O, CO_2, H_2, CO and O_2, the evolution of these species has to be modeled in a char conversion model to predict accurate char conversion rates. The governing equation for gas phase species is listed in Table 1. The corresponding source terms due to char conversion are

$$\dot{\omega}_{\mathrm{CO}} = 2\dot{\omega}_{\mathrm{oxid}}\frac{MW_{\mathrm{CO}}}{MW_{\mathrm{O_2}}} + f_{\mathrm{CO}}\dot{\omega}_{\mathrm{k_1}} + g_{\mathrm{CO}}\dot{\omega}_{\mathrm{k_4}} + \dot{\omega}_{\mathrm{H_2O,gasif}}\frac{MW_{\mathrm{CO}}}{MW_{\mathrm{H_2O}}} + 2\dot{\omega}_{\mathrm{CO_2,gasif}}\frac{MW_{\mathrm{CO}}}{MW_{\mathrm{CO_2}}} - \dot{\omega}_{\mathrm{CO,oxid}} \tag{11}$$

$$\dot{\omega}_{\mathrm{O_2}} = -\dot{\omega}_{\mathrm{oxid}} - \dot{\omega}_{\mathrm{CO,oxid}}\frac{1MW_{\mathrm{O_2}}}{2MW_{\mathrm{CO}}} \tag{12}$$

$$\dot{\omega}_{\mathrm{H_2}} = f_{\mathrm{H_2}}\dot{\omega}_{\mathrm{k_1}} + g_{\mathrm{H_2}}\dot{\omega}_{\mathrm{k_4}} + \dot{\omega}_{\mathrm{H_2O,gasif}}\frac{MW_{\mathrm{H_2}}}{MW_{\mathrm{H_2O}}} \tag{13}$$

This is the accepted version of an article published in Energy and Fuels
DOI: 10.1021/acs.energyfuels.8b00777

$$\dot{\omega}_{\mathrm{H_2O,g}} = \dot{\omega}_{\mathrm{evap}} - \dot{\omega}_{\mathrm{H_2O,gasif}} + f_{\mathrm{H_2O}}\dot{\omega}_{\mathrm{k_1}} + g_{\mathrm{H_2O}}\dot{\omega}_{\mathrm{k_4}} \tag{14}$$

$$\dot{\omega}_{\mathrm{CO_2}} = f_{\mathrm{CO_2}}\dot{\omega}_{\mathrm{k_1}} + g_{\mathrm{CO_2}}\dot{\omega}_{\mathrm{k_4}} - \dot{\omega}_{\mathrm{CO_2,gasif}} + \dot{\omega}_{\mathrm{CO,oxid}}\frac{MW_{\mathrm{CO_2}}}{MW_{\mathrm{CO}}} \tag{15}$$

$$\dot{\omega}_{\mathrm{tar}} = \dot{\omega}_{k_2} - \dot{\omega}_{k_4} - \dot{\omega}_{k_5} \tag{16}$$

where $\dot{\omega}_{k_4}$ represents reaction rates due to the tar cracking to non-condensable gases,

$$\dot{\omega}_{\mathrm{k_4}} = k_4 \rho^{\mathrm{g}}_{\mathrm{tar}} \epsilon_{\mathrm{g}}. \tag{17}$$

The fractions $f_{\mathrm{CO_2}}$, f_{CO}, $f_{\mathrm{H_2}}$ and $f_{\mathrm{H_2O}}$ define how much carbon dioxide, carbon monoxide, hydrogen and water vapor are produced from primary devolatilization reactions, and the fractions $g_{\mathrm{CO_2}}$, g_{CO}, $g_{\mathrm{H_2}}$ and $g_{\mathrm{H_2O}}$ define how much of the corresponding species are formed from tar reactions.

Homogeneous gas phase reactions are partly considered in this model, where carbon monoxide reactions occur inside the pores. This is a critical aspect that needs to be considered, since this reaction consumes oxygen and therefore even further restricts the oxygen transportation to the active sites. The corresponding reaction and kinetics that were used, are listed in Table 4.

Finally, the temperature equation becomes

$$\begin{aligned}\Big(\rho_{\mathrm{wood}}c_{P,\mathrm{wood}} + \rho_{\mathrm{char}}c_{P,\mathrm{char}} + \rho_{\mathrm{ash}}c_{P,\mathrm{ash}} + \rho_{\mathrm{l}}c_{P,\mathrm{l}} + \rho_{\mathrm{b}}c_{P,\mathrm{b}} + \epsilon_{\mathrm{g}}\rho^{\mathrm{g}}_{\mathrm{g}}c_{P,\mathrm{g}}\Big)\frac{\partial T}{\partial t} + \\ \Big(\rho_{\mathrm{l}}c_{\mathrm{P,l}}u_{\mathrm{l}} + \rho_{\mathrm{b}}c_{\mathrm{P,b}}u_{\mathrm{b}} + \epsilon_{\mathrm{g}}\rho^{\mathrm{g}}_{\mathrm{g}}c_{\mathrm{P,g}}u_{\mathrm{r}}\Big)\frac{\partial T}{\partial r} = \\ \frac{1}{r}\frac{\partial}{\partial r}\Big(r\lambda_{\mathrm{eff}}\Big(\frac{\partial T}{\partial r}\Big)\Big) - \Phi_{\mathrm{heat}}\end{aligned} \tag{18}$$

This is the accepted version of an article published in Energy and Fuels
DOI: 10.1021/acs.energyfuels.8b00777

where

$$
\begin{aligned}
\Phi_{\text{heat}} = \dot{\omega}_{k1,k2,k3} \triangle h_{\text{devol},1} + \dot{\omega}_{k4,k5} \triangle h_{\text{devol},2} + \dot{\omega}_{\text{evap}} \triangle h_{\text{evap}} \\
+ \dot{\omega}_{\text{oxid}} \Omega_1 \frac{MW_C}{MW_{O_2}} \triangle h_{\text{oxid}} + \dot{\omega}_{\text{H}_2\text{O,gasif}} \Omega_2 \frac{MW_C}{MW_{H_2O}} \triangle h_{\text{H}_2\text{O,gasif}} \\
+ \dot{\omega}_{\text{CO}_2\text{,gasif}} \Omega_3 \frac{MW_C}{MW_{CO_2}} \triangle h_{\text{CO}_2\text{,gasif}} + \dot{\omega}_{\text{CO,oxid}} \triangle h_{\text{CO,oxid}} \\
+ \dot{\omega}_{k1} \Big(\int_{T_0}^{T} (c_{\text{P,wood}} - c_{\text{P,non-cond. gases}}) dT \Big) + \dot{\omega}_{k2} \Big(\int_{T_0}^{T} (c_{\text{P,wood}} - c_{\text{P,tar}}) dT \Big) \\
+ \dot{\omega}_{k3} \Big(\int_{T_0}^{T} (c_{\text{P,wood}} - c_{\text{P,char}}) dT \Big) \\
+ \dot{\omega}_{\text{evap}} \Big(\int_{T_0}^{T} (c_{\text{P,water}} - c_{\text{P,vapor}}) dT \Big) \\
+ (\dot{\omega}_{\text{H}_2\text{O,gasif}} + \dot{\omega}_{\text{oxid}} + \dot{\omega}_{\text{CO}_2\text{,gasif}}) \Big(\int_{T_0}^{T} (c_{\text{P,char}} - c_{\text{P,non-cond. gases}}) dT \Big) \\
+ \dot{\omega}_{k4} \Big(\int_{T_0}^{T} (c_{\text{P,tar}} - c_{\text{P,non-cond. gases}}) dT \Big) + \dot{\omega}_{k5} \Big(\int_{T_0}^{T} (c_{\text{P,tar}} - c_{\text{P,char}}) dT \Big)
\end{aligned}
\tag{19}
$$

The the average bound water mass flux $\rho_{\text{b}} u_{\text{b}}$, entering Eq. (18) needs to be defined as suggested by Grønli[21]

$$
\rho_{\text{b}} u_{\text{b}} = -D_{\text{b}} \frac{\partial \rho_{\text{b}}}{\partial r} \tag{20}
$$

under the assumption that wood density remains more or less constant within the wet wood zone, where bound water transportation is of relevance.

The set of differential and algebraic equations has to be solved by a suitable solver. A complication is that homogeneous gas phase reactions, such as carbon monoxide oxidation, are very stiff, which has to be considered when a suitable solver is chosen. In the current work we use the IDA solver, which is a part of the SUNDIALS software package,[26] and time integration is done by a backward differentiation formula (order 1 to 5, which as well defines the temporal order of accuracy). The convective terms are discretized by first order up-winding, while the diffusion terms in the transport equations use a second order central difference. The spatial discretization is therefore of first order accuracy. In this work, the term combustion refers to the sum of all stages of thermal conversion; namely drying,

This is the accepted version of an article published in Energy and Fuels
DOI: 10.1021/acs.energyfuels.8b00777

devolatilization and char conversion.

2.2 Boundary conditions

The boundary conditions for temperature and species mass fractions are given by [8]

$$\lambda_{\text{eff}} \frac{\partial T}{\partial r} = \epsilon_{\text{particle}} \sigma (T_{\text{wall}}^4 - T_{\text{surface}}^4) + h_{\text{c}} (T_{\text{gas}} - T_{\text{surface}}) \tag{21}$$

and

$$\epsilon_{\text{g}} D_{\text{eff}} \frac{\partial Y_k}{\partial r} = h_{\text{m}} (Y_{\infty,k} - Y_{\text{surface,k}}). \tag{22}$$

The heat and mass transfer coefficients, h_{c} and h_{m}, entering these boundary conditions have to be corrected due to the influence of exiting gases. This influence is often called the blowing effect or the Stefan flow effect. It is only valid to set heat and mass transfer coefficients to their uncorrected values (marked by subscript $_{,0}$ in the following) if $\dot{M}_{\text{total}} \to 0$, i.e.;

$$h_{\text{c,0}} = \lim_{\dot{M}_{\text{total}} \to 0} h_{\text{c}} \tag{23}$$

and

$$h_{\text{m,0}} = \lim_{\dot{M}_{\text{total}} \to 0} h_{\text{m}}. \tag{24}$$

where $\dot{M}_{\text{total}}$ is the total mass flux of gas species leaving the particle, being defined as

$$\dot{M}_{\text{total}} = \rho_{\text{g}}^{\text{g}} \epsilon_{\text{g}} u_{\text{r}}. \tag{25}$$

The uncorrected mass transfer coefficient (without the influence of the Stefan flow) are found from

$$h_{\text{m,0}} = \frac{D_{\text{AB}} Sh}{d_{\text{P}}} \tag{26}$$

This is the accepted version of an article published in Energy and Fuels
DOI: 10.1021/acs.energyfuels.8b00777

while the corresponding heat transfer coefficient is calculated as

$$h_{\mathrm{c},0} = \frac{\mathrm{Nu}\lambda_{\mathrm{g}}}{d_{\mathrm{p}}}. \tag{27}$$

Both Nu and Sh can be obtained from the Ranz-Marshall correlation[9]

$$Nu = 2 + 0.6Re^{0.5}Pr^{1/3} \tag{28}$$

and

$$Sh = 2 + 0.6Re^{0.5}Sc^{1/3}. \tag{29}$$

for this specific test case, since a near-spherical particle is modeled. The diffusivity is calculated from the following equation[27]

$$D_{\mathrm{AB}} = D_{\mathrm{AB,ref}}\left(\frac{T}{T_{\mathrm{ref}}}\right)^{1.75}, \tag{30}$$

with the reference diffusivity, $D_{\mathrm{AB,ref}} = 2 \times 10^{-5}$ m^2/s, being taken from Fatehi and Bai.[8] The thermal diffusivity of the gas phase (λ_{g}) is assumed constant and the value found in Table 3 is used.

The corrected heat and mass transfer coefficients are defined as[28]

$$h_{\mathrm{m}} = \frac{\dot{M}_{\mathrm{total}}}{\left(\exp\left(\frac{\dot{M}_{\mathrm{total}}}{h_{\mathrm{m},0}}\right) - 1\right)}. \tag{31}$$

Due to the analogy between heat and mass transfer a similar expression can be defined for the corrected heat transfer coefficient[28]

$$h_{\mathrm{c}} = \frac{\dot{M}_{\mathrm{total}}\bar{c_{\mathrm{P,g}}}}{\left(\exp\left(\frac{\dot{M}_{\mathrm{total}}\bar{c_{\mathrm{P,g}}}}{h_{\mathrm{c},0}}\right) - 1\right)}. \tag{32}$$

where $\bar{c_{\mathrm{P,g}}}$ is the mass averaged specific heat capacity of the gas phase.

This is the accepted version of an article published in Energy and Fuels
DOI: 10.1021/acs.energyfuels.8b00777

For model validation, the surrounding gas phase temperature was set to 1050 K and the furnace wall temperature was set to 1276 K. The pressure at the particle surface was equal to ambient pressure.

The particle moisture content was 40 % (wet basis), and a near-spherical particle with a diameter of 9.5 mm and an aspect ratio of 1 was tested. The authors emphasize that for more realistic combustion modeling of solid fuel conversion, a dynamic coupling between solid- and gas-phase is recommended. Only a dynamically coupled solid- and gas-phase model can accurately link for example a fluctuating radiative feedback of the flame to the solid and predict how this change in external heat source affects the heat-controlled phenomena occurring inside the wood particle during thermochemical wood degradation and combustion, e.g. the volatile release rate. For example ANSYS Fluent, which has well-established gas phase models, lacks the ability to describe single wood particle or log combustion. This shortcoming therefore requires the implementation of a solid phase model via user-defined functions. Even though the authors aim for the CFD implementation of their solid phase model via user-defined functions, the current status is a model written as a stand-alone code. This is the first step in the development of the entire simulation tool (gas and solid phase). Before the user-defined functions can be developed, the authors, however, found that it is crucial to validate the chemical and physical phenomena considered and implemented in the stand-alone code. This is done in order to assure that the solid phase model is a suitable modeling tool by itself, independent of whether it is linked to a gas phase model or not. Hence, it was not the scope of this work to develop the entire simulation tool, but rather to present the solid phase combustion model.

3 Numerical set-up

The data given in Table 3 were used for the simulations presented in this paper, i.e. for modeling combustion of a single thermally thick poplar particle. For simulating the combustion

This is the accepted version of an article published in Energy and Fuels
DOI: 10.1021/acs.energyfuels.8b00777

of a poplar particle Mehrabian et al.[9] based their simulations on the following proximate analysis: 48.1 wt.% d.b. C, 5.77 wt.% d.b. H, 45.53 wt.% d.b. O and 0.1 wt.% d.b. N. They furthermore assumed an ash content of 0.5 wt.% d.b. which was also assumed in this work. This ash content outlines that wood in general contains little ash.

This is the accepted version of an article published in Energy and Fuels
DOI: 10.1021/acs.energyfuels.8b00777

Table 3: Properties used as input values for the drying, devolatilization and char conversion model. The data is applied for poplar wood (hardwood).

Property	**Unit**	**Value**	**Ref.**
Apparente/true wood density, (ρ_{wood} & $\rho_{\text{wood,true}}$)	[kg/m^3]	570 & 1500 ($\rightarrow \epsilon_{\text{pore},0} = 0.62$)	[1)] & [29]
Thermal conductivity (wood), $\lambda_{\text{wood},\parallel}$ \ $\lambda_{\text{wood},\perp}$	[W/(mK)]	0.73 \0.52	[7]
Thermal conductivity (ash), $\lambda_{\text{ash},\parallel,\perp}$	[W/(mK)]	1.03	[27]
Thermal conductivity (char), $\lambda_{\text{char},\parallel,\perp}$	[W/(mK)]	$1.47 + 1.1 \times 10^{-3}$ T	[27]
Thermal conductivity (gases), λ_{g}	[W/(mK)]	25.77×10^{-3}	[19]
Thermal conductivity (water), λ_{l}	[W/(mK)]	$0.278 + 1.11 \times 10^{-3}$ T	[7]
Bridge factor, ξ	[-]	0.68	[30]
Specific heat capacity (wood), $c_{\text{P, wood}}$	[J/(kgK)]	1500 + T	[9]
Specific heat capacity (ash), $c_{\text{P, ash}}$	[J/(kgK)]	754 + 0.586 (T - 273)	[27]
Specific heat capacity (non-condensable gases), $c_{\text{P, g}}$	[J/(kgK)]	$770 + 0.624$ T - 1.91×10^{-4} T^2	[21]
Specific heat capacity (char), $c_{\text{P, char}}$	[J/(kgK)]	$420 + 2.09$ T + 6.85×10^{-4} T^2	[21]
Specific heat capacity (tar), $c_{\text{P, tar}}$	[J/(kgK)]	$-100 + 4.4$ T -1.57×10^{-3} T^2	[21]
Specific heat capacity (vapor), $c_{\text{P, vapor}}$	[J/(kgK)]	$1670 + 6.4 \times 10^{-1}$ T	[21]
Permeability, $\kappa_{\text{solid }\perp,\ \parallel}$	m^2	10^{-14}	[31]
Particle emissivity, $\epsilon_{\text{particle}}$	[-]	0.85	[9]

[1)] This value was calculated based on knowing the apparent density and the true density.

The pre-exponential factors, activation energies and heat of reactions that were used for drying, devolatilization and char conversion are presented in Table 4. The kinetic data for

This is the accepted version of an article published in Energy and Fuels
DOI: 10.1021/acs.energyfuels.8b00777

248 evaporation modeling is only relevant if the kinetic rate drying model is used.

Table 4: Kinetic data used for modeling drying, devolatilization and char gasification and oxidation. *"Gases"* in the following table refer to non-condensable gases.

Reaction rate constant	Reaction	Pre-exponential factor [1/s]	Activation energy [kJ/mol]	Ref.	Heat of reaction [kJ/kg]	Ref.
k_1	Wood → Gases	1.11×10^{11}	177	[32]	-418	[33]
k_2	Wood → Tar	9.28×10^{9}	149	[32]	-418	[33]
k_3	Wood → Char	3.05×10^{7}	125	[32]	-418	[33]
k_4	Tar → Gases	4.28×10^{6}	107.5	[34]	42	[35]
k_5	Tar → Char	1×10^{5}	107.5	[36]	42	[35]
k_{evap}	$\rho_b \rightarrow \epsilon_g \rho_g^g Y_{vap}$	5.13×10^{10}	88	[37]	-2440	[5]
k_{oxid}	C + 0.5 O_2 → CO	1.715 T	74.8	[7]	9212	[1)]
$k_{H_2O,gasif}$	C + H_2O → CO + H_2	3.42 T	130	[5]	-10940	[1)]
$k_{CO_2,gasif}$	C + CO_2 → 2 CO	3.42 T	130	[5]	-14370	[1)]
$k_{CO,oxid}$	CO + 0.5O_2 → CO_2	$10^{12.35}$	167	[5]	10110	[5]

249 [1)] The heat of reactions have been calculated by assuming char reacting as pure C.

250 Hydrogen oxidation reactions are deactivated in the presented test runs, since it is as-
251 sumed that only minor amounts of hydrogen are formed from primary and secondary de-
252 volatilization. Since also steam gasification reactions are very slow compared to oxidation
253 reactions, the source of hydrogen is limited, also limiting the homogeneous oxidation reac-
254 tions.

255 In fact homogeneous oxidation reactions were only modeled for CO, neglecting that dur-

This is the accepted version of an article published in Energy and Fuels
DOI: 10.1021/acs.energyfuels.8b00777

ing devolatilization also other combustible gas products are formed. Theoretically all combustible gases formed during devolatilization, including CO, can contribute to homogeneous gas phase combustion within the pores. One expects CO, CO_2, H_2, CH_4 and some other short-chained hydocarbons (C_xH_y) as main products. Neves et al.[38] found, based on reviewing literature data and developing a model to predict the gas product yields, that the amounts of CH_4 and C_xH_y are commonly negligible for devolatilization at primary devolatilization temperatures (commonly below 500°C). For non-condensable gas formation occuring at these temperatures, CH_4 and C_xH_y mass fractions together form a contribution of 1% of the total non-condensable gas phase product yield. Only if the temperatures increase from 500°C to 850°C the sum of the two species forms a significantly higher contribution of 10%. However, then again this implies, that this increased formation of CH_4 and C_xH_y at higher temperatures than 500°C is due to secondary tar cracking reactions.[38] Other non-condensable gas phase products are even more restricted in their contribution to the total non-condensable gas phase yield (e.g. H_2 mass fraction only increased from 0.2% to less than 1% when temperature rose from 500°C to about 850°C).

Therefore the authors assumed that CO will be the main gas component that homogeneously consumes oxygen. Again emphasis is made that the detailed species composition of the product gas is not a modeling aim in the current work. The aim is the consideration of oxygen availability limitation for heterogeneous oxidation, not only by mass-transfer limitations but also chemical phenomena due to leaving gas products.

4 Model validation

The model was validated against experimental work by Lu et al.[5] These experimental data were for near-spherical particles with an aspect ratio of 1, and therefore also such particles were used for the model validation. However, their experimental results show a large spread. This indicates that the error-bars associated with the measurements, in particular of the

This is the accepted version of an article published in Energy and Fuels
DOI: 10.1021/acs.energyfuels.8b00777

temperature at the particle surface and in the particle center, were significant. This highlights how difficult it is to measure the temperature during char conversion, which is partly due to the ongoing size reduction of the particle during combustion.[5] Therefore, in order to validate the model, the modeling results of our 1D mesh-based model were not only compared against the experimental results but also against the modeling results by Lu et al.[5] and Fatehi and Bai.[8] Overall good agreement was found between our work and the work by Lu et al.[5] and Fatehi and Bai.[8] Small deviations are visible though, since some assumptions are different:

1. The specific heat capacities of wood, char, ash and gases are different. The reason is that it is not clear from the paper of Lu et al.[5] how the specific heat capacities for wood and char were chosen.

2. The porosity was allowed to change from wood ($\epsilon_{\mathrm{g}} = 0.62$) to char ($\epsilon_{\mathrm{char}} = 0.9$) to ash ($\epsilon_{\mathrm{ash}} = 0.9$, taken from Mehrabian et al.[9]). The authors assumed in this work that there is no change in porosity from char to ash (similar to what has been assumed by Fatehi and Bai[39]). When setting the initial wood porosity to 0.62, the true wood density has to be set to 1500 kg/m^3, in order to result in an apparent wood density of 570 kg/m^3. This is a reasonable assumption for true wood density of softwoods and hardwoods.[29] The assumed porosity by Lu et al.[5] ($\epsilon_{\mathrm{g}} = 0.4$) was considered too low, as it would require a true wood density of 950 kg/m^3, which is too low for most wood species. Therefore, different porosities were used in this work.

3. The diffusivity of gases was assumed to be temperature-dependent as suggested by Hermansson and Thunman.[27] This is in contrast to the constant diffusivity, equal to the one at room temperature, that was used by Lu et al.[5]

4. The model presented in this work is considering that liquid free water occupies part of the pore volume. This means that as long as liquid free water is present in the pores the volume fraction of the gas phase, is lower than the porosity. This is not commonly done in other works, e.g. Fatehi and Bai[8] and Lu et al.,[5] where the simplifying assumption

This is the accepted version of an article published in Energy and Fuels
DOI: 10.1021/acs.energyfuels.8b00777

is made that all liquid water present in the particle is embedded in the solid matrix and is therefore not hindering the gas phase flow.

5. Shrinkage is modeled based on the same concept as suggested by Lu et al.,[5] but shrinkage during drying was only considered if a change in bound water density occurred. A change in liquid free water density, due to liquid water evaporation, is not coupled to volumetric shrinkage. Therefore the empirical correlation describing shrinkage is given by[5]

$$\frac{V_{\text{particle}}}{V_{\text{particle},0}} = 1 + (1 - \beta_{\text{evap}})\Big(\frac{\rho_{\text{b}}}{\rho_{\text{b},0}} - 1\Big) + (1 - \beta_{\text{devol}})\Big(\frac{\rho_{\text{wood}}}{\rho_{\text{wood},0}} - 1\Big), \tag{33}$$

with β_{evap} being 0.9 for modeling shrinkage during drying, β_{devol} being 0.9 for modeling shrinkage during devolatilization. Volumetric shrinkage during char conversion has not been modeled since we assumed that the particle size reduction during char conversion is due to char consumption reactions and not volumetric shrinkage. The char particle size reduction, is instead accounted for by char being converted to ash at the outer part of the char layer.

6. Due to numerical instabilities obtained with higher specific surface areas and therefore stiffer char oxidation reactions, the authors assumed a reduction in actual specific surface area as conversion proceeded. This was done for purely numerical reasons. The influence of such a reduction was tested to be minor, not affecting the mass loss trends, while only slightly affecting the predicted char layer thickness. The actual specific surface area was assumed to be in the range of 10^4 to 10^5 m^2/m^3.

Considering that some assumptions were different, the modeling results were compared against modeling results by Fatehi and Bai[8] as well as Lu et al.,[5] to see if the model developed by the authors predicted similar temperatures and mass losses.

This is the accepted version of an article published in Energy and Fuels
DOI: 10.1021/acs.energyfuels.8b00777

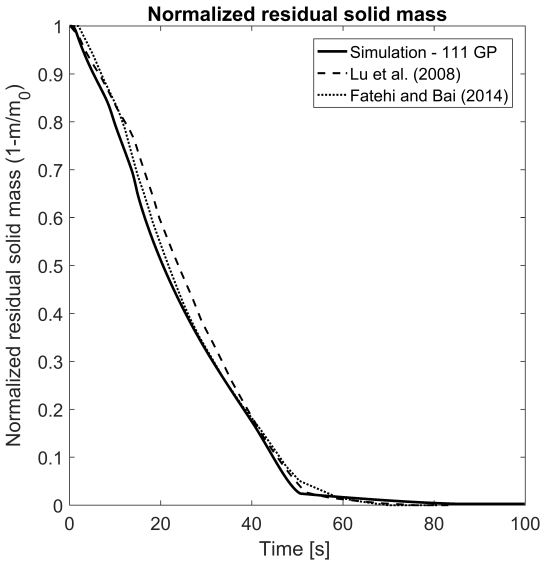

(a) Normalized residual solid mass prediction validated against other modeling results (Fatehi and Bai,[8] Lu et al.[5]).

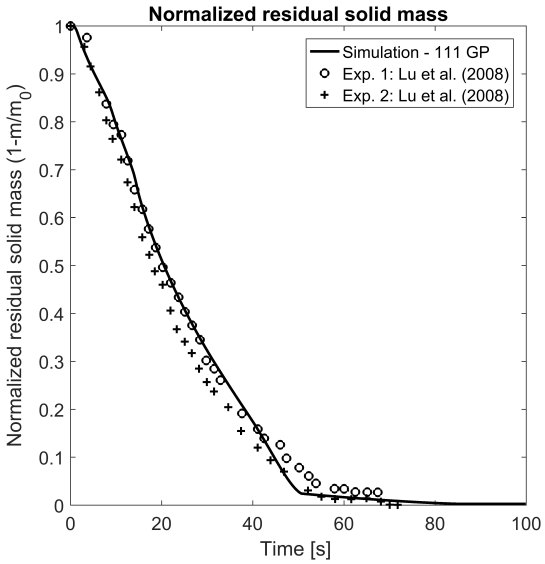

(b) Normalized residual solid mass prediction validated against experimental results by Lu et al.[5]

Figure 1: Validation of the normalized residual solid mass modeling results.

The normalized residual solid mass is very well predicted by the model (see Figure 1). Small deviations from experiments (Figure 1b) are linked to modeling assumptions, but the difference is rather negligible. The small deviations from other modeling works (see Figure 1a) are related to different assumptions, as listed in the beginning of the chapter. The model predicts a slightly longer conversion time compared to what has been found in experiments or other modeling works, which highlights that other thermophysical properties could be tested as well, to see how signficant their effect is on model accuracy and if other values are more suitable for describing poplar wood. When plotting the center and surface temperatures, more significant deviations became apparent (see Figure 2).

However, it needs to be pointed out that comparison of mass loss modeling results to experimental observations might be more reliable, since the measurement of temperature fields is more difficult than the continuous weighing of the residual particle.

This is the accepted version of an article published in Energy and Fuels
DOI: 10.1021/acs.energyfuels.8b00777

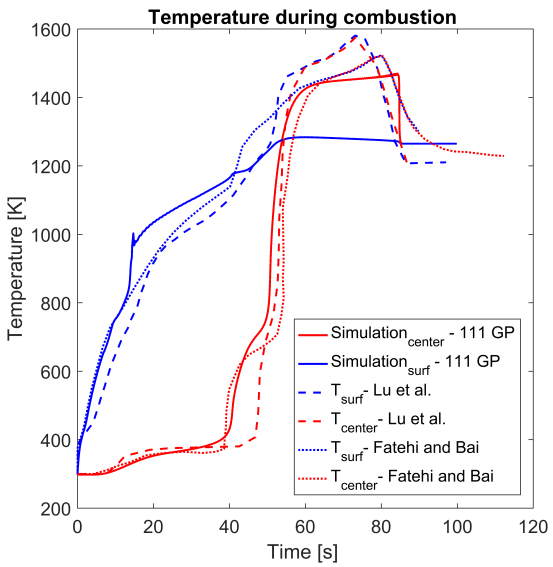

(a) Temperature modeling results validated against other modeling results (Fatehi and Bai,[8] Lu et al.[5]).

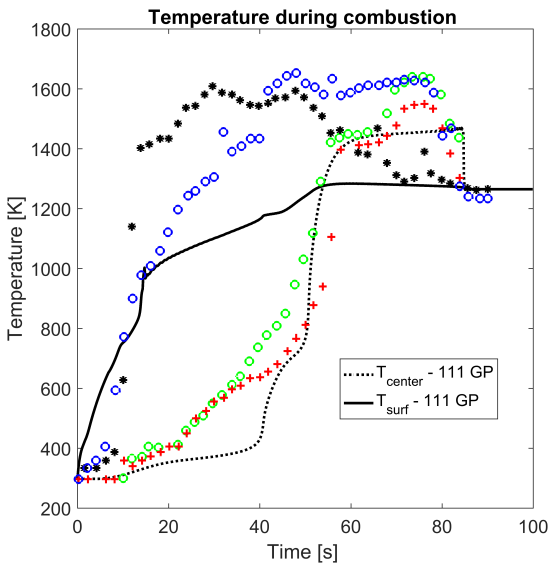

(b) Temperature modeling results validated against experimental results by Lu et al.[5]

Figure 2: Validation of the surface and center temperature modeling results. The red lines in Figure 2a are the predicted center temperatures and the blue lines are the predicted surface temperatures. The following symbols are used in Figure 2b: $T_{surface}$: ○ , ∗ ; T_{center}: ○ , + .

Drying can be identified in all modeling results by the temperature plateau at $\sim$ 373 K (see Figure 2a). The plateau in this model is not as obvious as shown by modeling results by Lu et al.,[5] which is due to different drying models. In this work a pure kinetic rate drying model is used while Lu et al.[5] used a combination of the thermal drying model and the kinetic rate drying model. This difference in drying models is due to the numerical set-up of this model, where liquid free water, evaporating by the thermal drying model, fills pores, while bound water, evaporating by the kinetic rate drying model, does not. Since Lu et al.[5] have not considered that liquid water as well occupies pore volume, even when using a combined thermal and kinetic rate drying model, it was found that the overall handling of the liquid phase is more similar to a pure bound water assumption in our model.

The center temperature increases quickly as soon as drying has been accomplished and only between 600 and 800 K the influence of endothermic primary devolatilization reactions seems to slow down the temperature increase, before finally the char oxidation reactions

This is the accepted version of an article published in Energy and Fuels
DOI: 10.1021/acs.energyfuels.8b00777

start contributing to the temperature increase. The extent to which this second temperature plateau between 600 and 800 K is visible depends on the choice of heat of reaction of the primary devolatilization reactions.

The predicted surface temperature differs significantly from the experimental data (Figure 2b), but as mentioned earlier, the deviation between the two experimental series is also significant. Further validation against other experimental data is challenging since there is little information available in the open literature that covers experiments of single wood particles and logs converting under similar conditions, where the full thermal conversion is included. The predicted surface temperature also deviated from the predicted surface temperature by Lu et al.[5] and Fatehi and Bai.[8] It is assumed that this difference is due to assumed wood properties, such as e.g. porosities, emissivity.

Overall, it was found that the modeling results of the wood combustion model differ from experimental results when it comes to center and surface temperature predictions. However, the mass loss predicted by the wood combustion model agrees well with what has been observed experimentally. Since temperature measurements are so challenging due to the size reduction of the char particle during char consumption and due to the intrusive nature of the measurements in the particle center, it is assumed that the deviation of modeling results from experimentally observed surface and center temperatures is mainly due to experimental artifacts. Measuring the mass loss, on the other hand, can still be accurately done, and with respect to that, the modeling results are very close to the experiments. This suggest that the model is of acceptable accuracy.

One expects that if the mass loss is accurate, also the gas release during drying, devolatilization and char conversion is accurately predicted. This is an important input value for the gas phase model (=input data entering the CFD platform).

Due to the relatively large differences between numerical and experimental predictions, it is clear that the surface temperature prediction has to be interpreted with care. Since the temperature is coupled to the gas phase model, an error in the solid phase model with respect

This is the accepted version of an article published in Energy and Fuels
DOI: 10.1021/acs.energyfuels.8b00777

to this temperature profile could potentially affect the results of a simulation tool for wood stove design and optimization. However, then again one has to point out that validation of this surface temperature is very challenging, since experiments are obviously affected by significant errors. Furthermore, the wood particle surface is very much simplified (evened out and therefore assumed ideal). In addition, catalytic effects of minerals are entirely neglected, which can affect char conversion, and as a consequence, also char oxidation and corresponding heat release. Furthermore, the char is simply assumed to be pure C instead of also considering that it will contain fractions of H and O.

4.1 Grid-independence study

Compared to the pure drying and devolatilization model, it is expected that a finer mesh is required when char oxidation and gasification reactions are included in the model. One reason for this is that steep temperature gradients are expected in the particle, since exothermic char oxidation starts at the surface of the particle while evaporation still occurs in the particle center. Steep gradients are also expected for the oxygen concentration in the particle. Oxygen diffusion into the particle is limited by oxygen-involving reactions at the char surface, or even by oxidation reactions of the exiting gases, such as CO. As a consequence, the oxygen cannot diffuse much into the particle, which means that the oxygen content is significant only in the vicinity of the char surface.

Therefore, as part of the model development, the authors tested mesh refinement, to see how fine the mesh has to be to yield a grid-independent solution, and how coarse it can be to yield numerically efficient modeling tools.

It was found that a mesh with 13 grid points is not yielding grid-independent solutions. One can clearly see peaks in the surface temperature predictions, which are purely numerical and result from the rather coarse mesh. Furthermore, the thermochemical conversion is predicted too fast, since full conversion is achieved at earlier times compared to finer meshes with 27, 55 and 111 grid points. Therefore, further grid refinement was tested and meshes

This is the accepted version of an article published in Energy and Fuels
DOI: 10.1021/acs.energyfuels.8b00777

of 27, 55 and 111 grid points were studied. It was found that there was only a minor difference in modeling results between a mesh with 55 and with 111 grid points. Therefore, it is assumed that grid-independent results can already be obtained with a mesh of 55 grid points, which at the same time requires lower computational cost compared to a mesh with 111 grid points. The mesh with 27 grid points still resulted in some deviation in normalized mass prediction as well as temperature predictions compared to the very fine meshes of 55 and 111 grid points but the overall prediction of conversion trends and temperature trends was similar to what has been obtained from very fine meshes of 55 and 111 grid points. For qualitatively studying the conservation trends, a mesh woth 27 can as well be used.

The relative error in mass conservation for a mesh of 55 grid points was 1.93 % and for a mesh of 111 grid points it was 1.94 %. This highlights that since mass is well conserved with both meshes, a grid with 55 grid points, can be used for studying the combustion behavior of the particle tested in this paper.

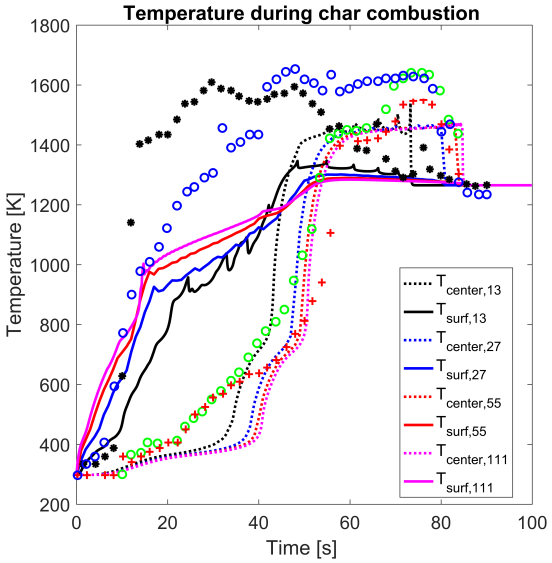

(a) Temperature evolution obtained with a mesh of 13, 27, 55 and 111 grid points along the particle radius. The experimental data from Lu et al.[5] for surface and center temperatures are plotted and the corresponding symbols are: $T_{surface}$: $*$ and $\circ$; T_{center}: $+$ and $\circ$.

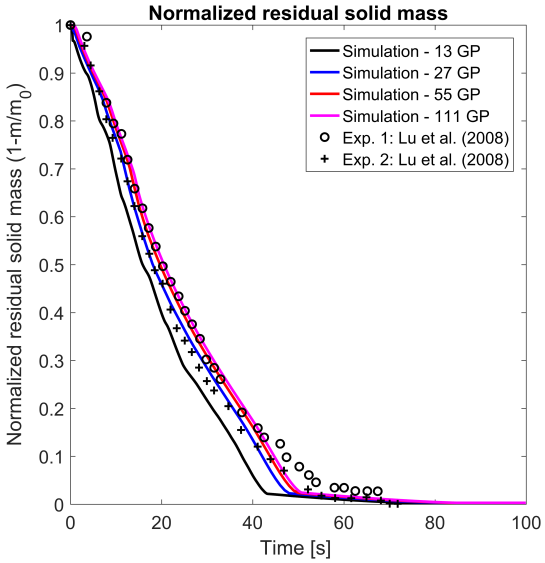

(b) Normalized residual solid mass evolution obtained with a mesh of 13, 27, 55 and 111 grid points along the particle radius.

Figure 3: Effect of the grid point number on modeling results.

This is the accepted version of an article published in Energy and Fuels
DOI: 10.1021/acs.energyfuels.8b00777

The conclusion that grid-independent results are obtained with 55 grid points is furthermore supported by the difference between temperature and oxygen mass fraction predictions (Figure 4). The differences obtained with meshes of 55 and 111 grid points are negligible. On the other hand one can clearly see that predictions obtained with a mesh of 13 grid points, deviate significantly, from predictions obtained from finer meshes.

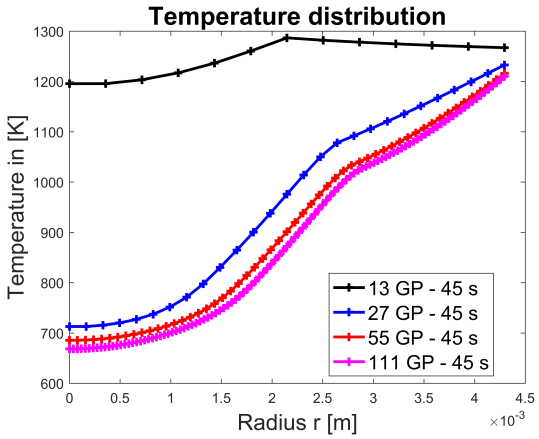

(a) Temperature distribution for meshes composed of 13, 27, 55 and 111 grid points.

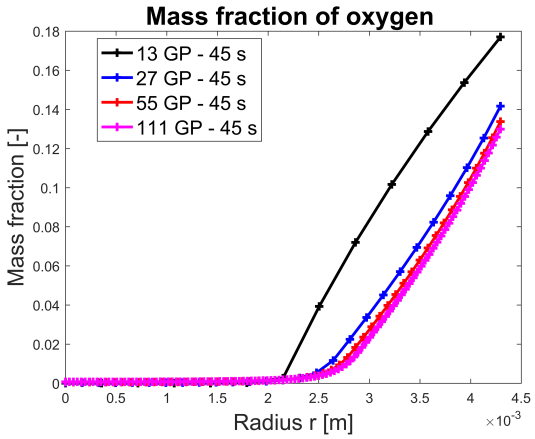

(b) Predicted oxygen mass fraction distribution for meshes composed of 13, 27, 55 and 111 grid points.

Figure 4: Effect of grid point number on the modeling results for temperature and oxygen mass fraction distribution within the reacting single particle.

It seems that the coarser meshes (13 and 27 grid points) predict slightly different times at which different stages of thermochemical conversion begin (Figure 5). Furthermore the char oxidation rate predicted with a mesh of 13 grid points, does not show a realistic physical behavior. Significant numerical oscillations are visible and are only due to the coarse mesh. Reduced numerical oscillations can even still be observed with a grid of 27 mesh points. The differences between the reaction rates predicted with 55, and 111 grid points on the other hand are minor.

This is the accepted version of an article published in Energy and Fuels
DOI: 10.1021/acs.energyfuels.8b00777

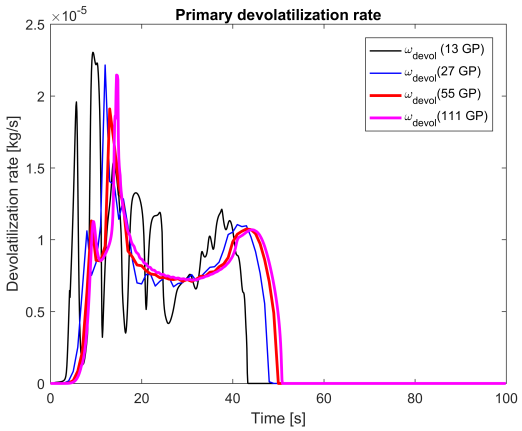

(a) Primary devolatilization rates as a function of time.

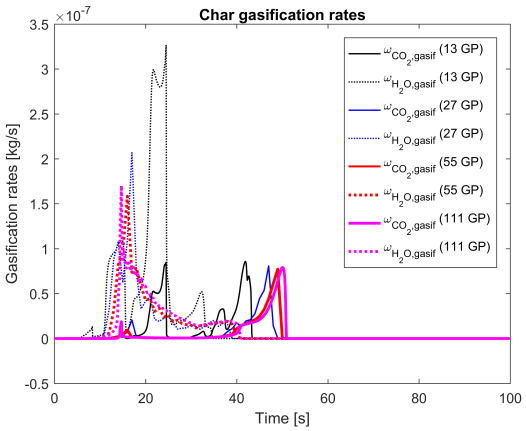

(b) Gasification rates as a function of time.

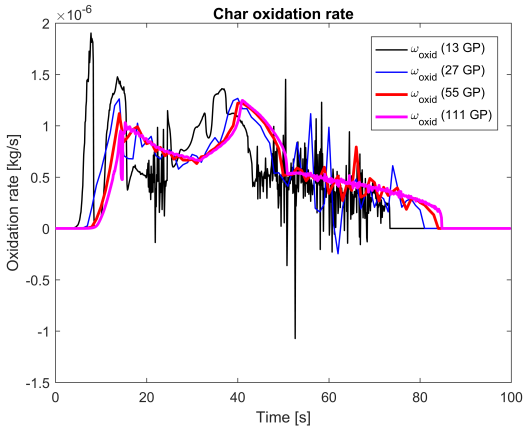

(c) Char oxidation rates as a function of time.

Figure 5: Grid-independence study with respect to reaction rates as a function of time during single wood particle combustion. Grid refinement was done from the originally coarse mesh of 13 grid points (spanning over the particle radius) to 27, 55 and 111 grid points.

When comparing the reaction rates, one can identify that again the difference between the predicted reaction rates obtained with meshes of 55 and 111 grid points is minor which again supports the conclusion that a mesh of 55 grid points is sufficient to yield grid-independent solutions.

This is the accepted version of an article published in Energy and Fuels
DOI: 10.1021/acs.energyfuels.8b00777

5 Results and discussion

In this section we will first give a detailed presentation of the conversion process of a thermally thick wood particle. Then, we will discuss the effect of particle size on the thermal conversion, and in particular on the position and extent of the conversion zones.

It has been stated in the literature that volatiles release from biomass occurs in three stages, with 10 % of the volatiles being released between 200 and 300 °C, 70 % between 300 and 400 °C and the remaining 20 % between 400 and 900 °C.[14] This, compared to the evaporation at about 100 °C, implies that a very broad temperature range, and therefore a larger number of grid points, is included in the primary devolatilization zone of wood.

Char conversion is the slowest stage of the entire thermal wood conversion, as oxygen diffusion to the active sites is limited. As oxygen cannot penetrate far into the particle, the char conversion occurs in a relatively thin zone.

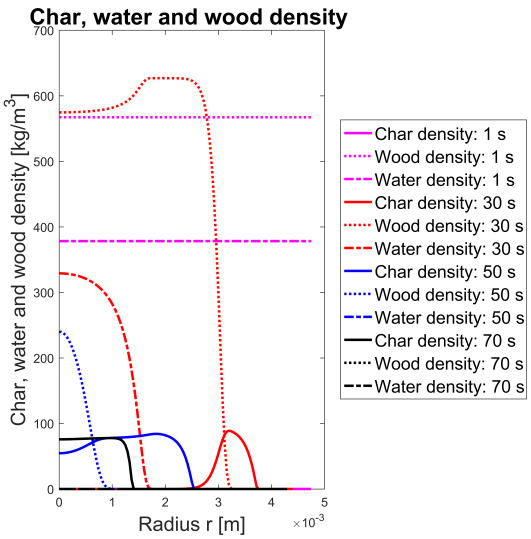

Figure 6: Char, wood and liquid water density at different times during thermal conversion.

One can identify the different conversion zones by the gradients of either liquid water, wood or char. Figure 6 clearly shows that the theoretically narrow drying zone is smeared over some grid points in this model (see water density at 30 s). This smearing is due to the application of the kinetic rate drying model, which models drying over a broader temperature

This is the accepted version of an article published in Energy and Fuels
DOI: 10.1021/acs.energyfuels.8b00777

447 range than at exactly 100 °C.

448 When studying the reaction rates in Figure 5 (for the 55 grid points test case), one can see
449 that the reaction rates are enhanced at different times. The first peak of the devolatilization
450 rate (at about 10 s) is due to very fast heating of the near surface areas of the particle.
451 Since devolatilization is heat transfer controlled, the fast heating of the outer zones leads to
452 a sudden and significant start of devolatilization. After this initial phase, the heat transfer
453 further inward is slower due to the build-up of an insulating char layer outside the dry wood
454 and due to the increased blowing effect that results from the production of volatile gases.
455 This reduced heat transfer to the dry wood, yields a slow-down of devolatilization. The
456 second increase in the devolatilization rate (around 15 s) is due to enhanced heat release
457 due to exothermic CO oxidation reactions as well as exothermic char oxidation reactions.
458 Char gasification starts slightly after char oxidation reactions as well as CO oxidation, since
459 gasification reactions are slower. The drop after the second increase is assumingly due to
460 the decreasing heating contribution of char oxidation and CO oxidation reactions. The
461 devolatilization zone moves further away from the char conversion zone and therefore a more
462 limited influence of the heat release in the char conversion zone on the heat transfer controlled
463 devolatilization zone occurs. In fact, it was found that a change in temperature gradient
464 due to the enhanced contribution of exothermic reactions can have a significant influence on
465 the devolatilization rate, since the reaction rates (especially for the reaction of wood to tar)
466 increase significantly as soon as higher temperatures are reached.

467 It was found that CO oxidation reactions influence wood particle combustion in two ways.
468 Firstly, heterogeneous oxidation reactions slow down, since the oxygen diffusing inward is
469 also consumed by the CO. Secondly, the heat release due to CO oxidation results in an
470 acceleration of heat transfer controlled processes.

471 Compared to char oxidation (see Figure 5c), steam and CO_2 gasification are significantly
472 slower (see Figure 5b). This was evaluated by comparing the maximum values for steam and
473 CO_2 gasification and oxidation reaction rates.

This is the accepted version of an article published in Energy and Fuels
DOI: 10.1021/acs.energyfuels.8b00777

Figure 6 shows that the particle, with an initial diameter of 9.5 mm, decreases to about 8.58 mm in 70 s. This means that the model predicts only limited shrinkage. One can, however, see a very thick ash layer building up. At 70 s, the char core is only about 2.8 mm in diameter, while the full particle is still about 8.58 mm. This suggests that the current model cannot very well describe particle size reduction for wood, since for low-ash biomass, such as wood, one expect that the ash will immediately fall off the residual char core instead of building up an ash layer. A signficant influence of ash seems more reasonable for high-ash content biomass, such as straw.

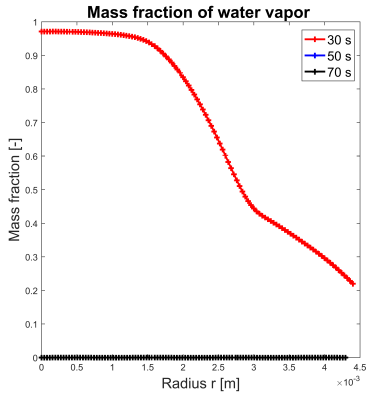

(a) Water vapor mass fraction at different times during wood particle combustion.

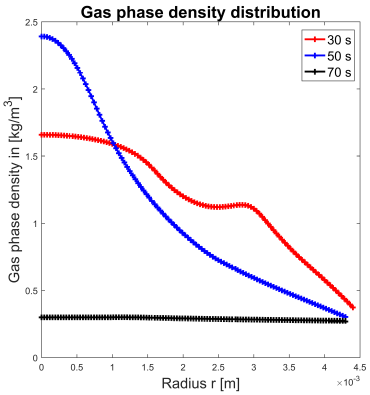

(b) Gas phase density at different times during wood particle combustion.

Figure 7: Water vapor mass fraction and gas phase density at different times during wood particle combustion.

As long as drying is still occurring, the mass fraction of water vapor inside the porous wood particle is high (see 30 s in Figure 7a). After the drying is finalized in the wood particle center, the water vapor is quickly transported outward. During the thermal conversion it seems that only very little water vapor is consumed by steam gasification reactions, since these reactions are slow (see Figure 5b).

The gas density is rather high in the particle center during the drying and devolatilization phases (see Figure 7b). A significant amount of organic mass is entering the gas phase during wood devolatilization. Similarly, a lot of water vapor is quickly released to the gas phase during drying. Both phenomena result in higher gas density. The shown gas phase density

This is the accepted version of an article published in Energy and Fuels
DOI: 10.1021/acs.energyfuels.8b00777

profile leads to a pressure peak in the particle center. The pressure drops to ambient pressure at the particle surface. This gas phase pressure gradient is the driving force for gas phase convection.

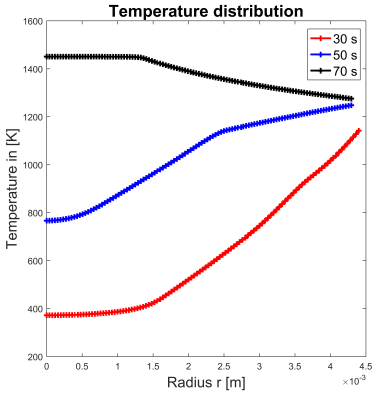

(a) Temperature at different times during thermal conversion.

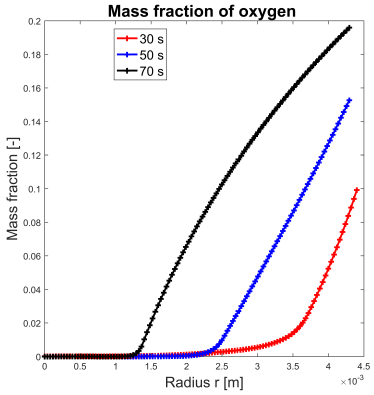

(b) Oxygen mass fraction at different times during thermal conversion.

Figure 8: Temperature and oxygen mass fraction modeling results at different times during wood particle thermal conversion.

In Figure 8 it is shown that after devolatilization is finalized, the oxidation of the residual char leads to a temperature increase (see temperature at 70 s), which is even exceeding the furnace temperature. This heat is then conducted outward through the ash-layer, while the temperature drops from more than 1400 K to a surface temperature slightly above the furnace temperature. Cooling of the particle at this stage of thermal conversion occurs via radiative losses.

Figure 8b shows that the oxygen mass fraction is more or less zero within the char core. In fact, oxygen diffusion into the char part of the particle is limited, as can be seen when comparing the size of the char core and the oxygen mass fraction at 70 s. The oxygen mass fraction at the outer particle surface quickly increases from 10 % at 30 s to almost 20 % at 70 s, which is due to reduced blowing factors. After devolatilization is over, the outwardly directed flow of gas is limited. This minimizes the blowing effect and, hence, increases the mass transfer coefficient.

Tar is produced during devolatilization, which can be seen from the tar mass fraction at

This is the accepted version of an article published in Energy and Fuels
DOI: 10.1021/acs.energyfuels.8b00777

30 and 50 s in Figure 9a. The tar is then consumed by secondary tar reactions on its way through the surrounding char layer.

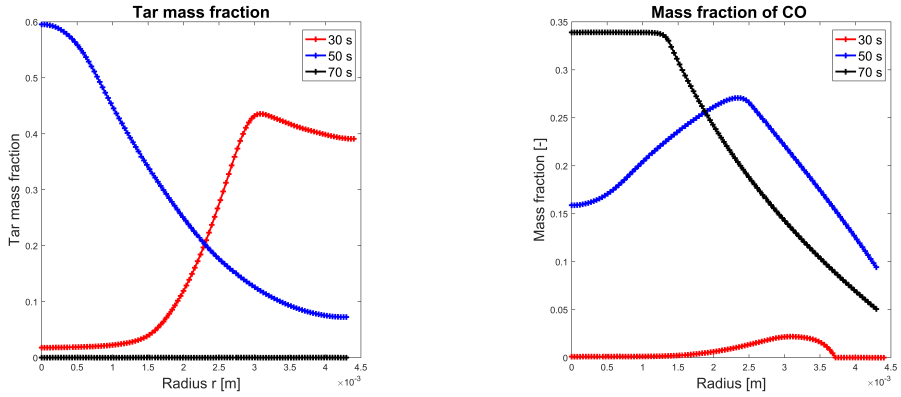

(a) Tar mass fraction at different times during combustion.

(b) CO mass fraction at different times during combustion.

Figure 9: CO and tar mass fraction modeling results at different times during wood particle combustion.

Figure 9b shows that the mass fraction of CO is low at early times, which is due to limited char oxidation reactions, while at 70 s, the CO mass fraction increases to a maximum of about 33%, which indicates that mainly char is converting. This implies that most of the CO is formed during char oxidation rather than primary or secondary devolatilization reactions. The CO mass fraction drops to zero towards the particle surface at 30 s. This is due to CO oxidation reactions. The drop to lower values toward the surface at 50 s and 70 s is due to inward diffusion of oxygen and nitrogen, since CO oxidation is negligible because of lack of water vapor due to the termination of the drying stage. Oxidation of CO require OH radicals in order to occur sufficiently fast. The OH radicals are supplied in sufficient quantities by the water vapor leaving the evaporating inner sections of the particle. In fact, the need for OH radicals for sufficiently fast CO oxidation reactions can be seen from [6]

$$\dot{\omega}_{\mathrm{CO}} = k_{\mathrm{CO}} \left(\frac{\epsilon \rho_{\mathrm{g}}^{\mathrm{g}} Y_{\mathrm{CO}}}{MW_{CO}} \right) \left(\frac{\epsilon \rho_{\mathrm{g}}^{\mathrm{g}} Y_{\mathrm{O_2}}}{MW_{O_2}} \right)^{0.25} \left(\frac{\epsilon \rho_{\mathrm{g}}^{\mathrm{g}} Y_{\mathrm{H_2O}}}{MW_{H_2O}} \right)^{0.5} MW_{CO}. \tag{34}$$

This is the accepted version of an article published in Energy and Fuels
DOI: 10.1021/acs.energyfuels.8b00777

5.1 The effect of wood particle size

In the following, we study the influence of different wood particle diameters on their combustion behavior. The wood particles tested in this work have an aspect ratio of 4, and due to their large diameter and their cylindrical shape they can rather be referred to as wood logs. It is assumed that within the size range modeled in this work, the char burnout time is not affected by either increased or reduced char reactivity due to different internal heat transfer rates. Only within the range of high heating rates of e.g 10^4°C/s one expects to see reduced char reactivty.[40–42]

The tested wood logs were of cylindrical shape with an aspect ratio of 4. The diameters and corresponding conversion times are listed in Table 5. The furnace wall temperature was 1276 K, with the surrounding gas phase temperature was kept at 1050 K.

This is the accepted version of an article published in Energy and Fuels
DOI: 10.1021/acs.energyfuels.8b00777

Table 5: List of tested wood log diameters and aspect ratios as well as conversion times. The water content was 40 wt% wet basis in all test cases. The particle diameter is expressed by d_{particle} and the wood log length is expressed by l_{particle}. The total thermal conversion time was defined as the time when 99 % of the initial wet wood log mass had been converted.

$\mathbf{d}_{\text{particle}}$	$\mathrm{l}_{\text{particle}}$	V	$\mathbf{t}_{\text{evap}}$	$\mathbf{t}_{\text{devol}}$	$\mathbf{t}_{\text{oxid}}$	$\mathbf{t}_{\text{CO}_2\text{,gasif}}$	$\mathbf{t}_{\text{H}_2\text{O,gasif}}$	$\mathbf{t}_{\text{total}}$
[mm]	[mm]	[mm^3]	[s]\%	[s]\%	[s]\%	[s]\%	[s]\%	[s]
10	40	3.14×10^{-6}	38\	51 \	67\	46 \	32\	72
			52.8	70.8	93.1	63.9	44.4	
20	80	2.513×10^{-5}	145 \	182\	292\	178\	143\	297
			48.8	61.3	98.3	60	48.1	
40	160	2.01×10^{-4}	526\	632\	1285\	610\	520\	1292
			40.7	48.9	99.5	47.2	40.2	

Table 5 shows that wood log size, and therefore also the wood log mass, have a significant influence on the duration of all conversion stages of a full combustion process.

The start of a conversion stage, i.e. drying, devolatilization or char conversion, is defined as the time when the reaction rates clearly start to increase. When the conversion rates drop to very small values again, the conversion stage is considered as being accomplished.

The corresponding plots have not been added to the paper, since they show the same trends as the reaction rates in Figure 5 and the most relevant information are summarized in Table 5.

It was observed that by increasing the wood log diameter by a factor of 2 (compared to the reference wood log diameter of 10 mm) the evaporation time increased by a factor of

This is the accepted version of an article published in Energy and Fuels
DOI: 10.1021/acs.energyfuels.8b00777

about 3.8, and the devolatilization time by a factor of 3.6. The char burnout time increased by a factor of 4.3. When comparing the time required for the full thermal conversion process, it is found that the full conversion time increased by a factor of 4.1. Even further increasing the particle size by increasing the wood log diameter by a factor of 4 (compared to the reference wood log diameter of 10 mm) prolonged the evaporation time by a factor of 13.8, while the devolatilization time was 12.4 times longer and the char burnout time was 19.2 times longer than in the reference case. The full thermal conversion process was prolonged by a factor of 17.9 compared to the thermal conversion time for a 10 mm wood log.

In order to compare the extents to which conversion zones are present at a given stage during thermal conversion, the authors compared the char, wood and liquid water densities at the time of conversion where 50 % of the inital wet wood mass have been converted. The results are found in Figure 10.

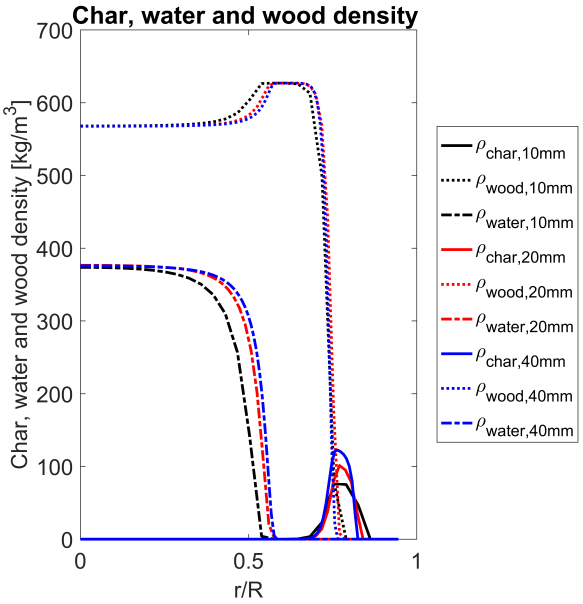

Figure 10: Conversion zones of cylindrical wood logs with diameters ranging from 10 mm to 40 mm and an aspect ratio of 4.

One can observe that for smaller particles, the peak of char density is lower than for larger particles, which is due to the different internal heat transfer rates. A lower internal heat transfer rate results in more char being formed. As a consequence, the wood log with

This is the accepted version of an article published in Energy and Fuels
DOI: 10.1021/acs.energyfuels.8b00777

a diameter of 10 mm has a maximum char density of 75 kg/m^3 at 50 % thermal conversion, while the largest wood log (d_P = 40 mm) has a maximum char density of 120 kg/m^3 at the same degree of conversion. The char conversion zone is defined by the drop of char density, from its maximum value to zero. The char conversion zone spreads over 10.8 % of the initial wood log radius for small wood logs (d_P=10 mm), while it spreads over a zone of 6 % of the initial radius for the large wood logs (d_P = 40 mm). In the wood log of intermediate size (d_P = 20 mm) the char conversion zone spread over 7 % of the initial wood log radius.

The extent to which the devolatilization zone is present, is decreasing as particle size increases. While the devolatilization zone spreads over 21.24 % of the initial radius for the small wood log (d_P = 10 mm), it spreads over 11.5 % of the radius of the large wood log (d_P = 40 mm).

For the drying zone this analysis is more challenging due to the smearing effect of the kinetic rate drying model. Therefore, an analysis of the extent to which the drying zone is present in the wood logs of different sizes, is rather rough. In order to avoid misinterpretation of the results, we defined the drying zone, as the zone where the liquid water density drop from 360 kg/m^3 to zero. By this, it was found that the extent to which the drying zone is present decreases as the wood log diameter increases. While the drying zone spreads over a range of 26 % of the initial wood log radius for small logs (d_P = 10 mm), it only spreads over 17.5 % for large logs (d_P = 40 mm).

The heat transfer controlled processes (drying and devolatilization) cover a larger domain of the particle than diffusion controlled char conversion.

It is interesting to see that the model, validated against a rather small near-spherical particle, can be up-scaled to signficantly larger particle dimensions (diameter in cm-range and aspect ratios larger than 1) and still replicate theoretically expected trends. This is a very promising observation, since only very limited literature is available on the thermochemical degradation of large wood logs, of sizes comparable to what is applied in wood stoves. Consequently, most of the model validation will have to be done against experiments done

This is the accepted version of an article published in Energy and Fuels
DOI: 10.1021/acs.energyfuels.8b00777

with small thermally thick particles. After validation the particle must be up-scaled, if one aims to develop a solid phase model for wood log combustion in domestic heating appliances.

The authors therefore conclude that this numerical model, can be used to describe wood particle conversion as well as large wood log combustion.

6 Conclusions and recommendations

The 1D model has proven to be a good approach to fundamentally study the combustion behavior of wood particles. Nonetheless, obtained temperature data requires further validation, despite accurate mass loss predictions. Accurate surface temperature predictions, is not possible with a stand-alone solid phase combustion model, since dynamic coupling between gas phase and solid phase is required to accurately predict wood particle surface temperatures. The current solid phase model seems to capture the relevant chemical and physical phenomena very well, suggesting that coupling it to a gas phase model, is a promising advancement for future research.

In this work, a combustion model for thermally thick wet near-spherical particles was validated and due to the assumption of thermally thick particles during validation, used for studying the combustion behavior of large wood logs. The model describes drying, devolatilization and char oxidation and gasification, as well as homogeneous oxidation reactions of CO. The model can describe oxygen diffusion into the particle, while accounting for a reduced mass transfer coefficient due to blowing of exiting gases. Volumetric shrinkage of the particle was considered during drying and devolatilization. Size reduction during char conversion was only considered by char conversion to pure ash at the outer char zone. Comparison to other modeling works and experimental data showed that the model is of acceptable accuracy and can be used for fundamental studies on combustion behavior of large thermally thick wood particles and logs.

It was shown that for a near-spherical particle (d_P=9.5 mm) a mesh of 55 grid points

This is the accepted version of an article published in Energy and Fuels
DOI: 10.1021/acs.energyfuels.8b00777

(spanning over the particle radius) results in grid-independent solutions for the current conditions. Furthermore, it was found that due to challenges related to surface temperature measurements of combusting wood particles, validation of models is hard.

The wood log size does not influences the relative position of the conversion zones. The relative volume over which the three conversion zones were present decreased with increasing wood log diameter.

The current shrinkage model cannot accurately describe the actual particle size of a near ash-free wood particle. For such wood species it is more accurate to assume inward moving boundaries, which means that no ash-layer builds up but that ash instead falls off immediately. With the current shrinkage model, a thick ash layer is allowed to build up. It is therefore recommended to compare the modeling results of a model with inward-moving boundary conditions, to the modeling results presented in this work and study which ash consideration is more appropriate for wood combustion modeling.

Furthermore, it needs to be mentioned, that with respect to model input data, such as wood properties, or even reaction kinetics, as well as char reactivity, noteable uncertainties do exist that will affect modeling results. Despite these potential sources of error, for the case studied here, the presented model has proven to capture physical and chemical phenomena related to combustion rather well. The sensitivity of the model to model input data should be studied in future works, in order to assure that the model predicts combustion of single wood particles under different conditions equally well. However, such an extensive parametric study was not within the scope of this work dealing with model development.

7 Acknowledgments

This work has been carried out within the WoodCFD (243752/E20) project, which is funded by: Dovre AS, Norsk Kleber AS, Jøtulgruppen and Morsø AS together with the Research Council of Norway through the ENERGIX program.

This is the accepted version of an article published in Energy and Fuels
DOI: 10.1021/acs.energyfuels.8b00777

References

(1) Yang, Y. B.; Sharifi, V. N.; Swithenbank, J.; Ma, L.; Darvell, L. I.; Jones, J. M.; Pourkashanian, M.; Williams, A. *Energy Fuels* **2008**, *22*, 306–316.

(2) Skreiberg, Ø.; Seljeskog, M.; Georges, L. *Chem. Eng. Trans.* **2015**, *43*, 433– 438.

(3) Porteiro, J.; Granada, E.; Collazo, J.; Patiño, D.; Morán, J. C. *Energy Fuels* **2007**, *21*, 3151–3159.

(4) Porteiro, J.; Míguez, J. L.; Granada, E.; Moran, J. C. *Fuel Process. Technol.* **2006**, *87*, 169–175.

(5) Lu, H.; Robert, W.; Peirce, G.; Ripa, B.; Baxter, L. L. *Energy Fuels* **2008**, *22*, 2826–2839.

(6) Lu, H. Experimental and modeling investigation of biomass particle combustion. PhD thesis, Brigham Young University, Provo, Utah, 2006.

(7) Thunman, H.; Leckner, B.; Niklasson, F.; Johnsson, F. *Combust. Flame* **2002**, *129*, 30–46.

(8) Fatehi, H.; Bai, X. S. *Combust. Sci. Technol.* **2014**, *186*, 574–593.

(9) Mehrabian, R.; Zahirovic, S.; Scharler, R.; Obernberger, I.; Kleditzsch, S.; Wirtz, S.; Scherer, V.; Lu, H.; Baxter, L. L. *Fuel Process. Technol.* **2012**, *95*, 96 – 108.

(10) Galgano, A.; Di Blasi, C.; Horvat, A.; Sinai, Y. *Energy Fuels* **2006**, *20*, 2223–2232.

(11) Galgano, A.; Di Blasi, C. *Prog. Comput. Fluid Dyn.* **2006**, *6*, 287–302.

(12) Haberle, I.; Skreiberg, Ø.; Łazar, J.; Haugen, N. E. L. *Prog. Energy Combust. Sci.* **2017**, *63*, 204 – 252.

This is the accepted version of an article published in Energy and Fuels
DOI: 10.1021/acs.energyfuels.8b00777

(13) Li, J.; Paul, M. C.; Younger, P. L.; Watson, I.; Hossain, M.; Welch, S. *Appl. Energy* **2015**, *156*, 749 – 755.

(14) Saeed, M.; Andrews, G.; Phylaktou, H.; Gibbs, B. *Fuel* **2016**, *181*, 347 – 357.

(15) Riaza, J.; Gibbins, J.; Chalmers, H. *Fuel* **2017**, *202*, 650 – 655.

(16) Pozzobon, V.; Salvador, S.; Bézian, J. J.; El-Hafi, M.; Maoult, Y. L.; Flamant, G. *Fuel Process. Technol.* **2014**, *128*, 319 – 330.

(17) Lu, Z.; Jian, J.; Jensen, P. A.; Wu, H.; Glarborg, P. *Energy Fuels* **2016**, *30*, 5772–5778.

(18) Haberle, I.; Haugen, N. E. L.; Skreiberg, Ø. *Energy Fuels* **2017**, *31*, 13743–13760.

(19) Di Blasi, C. *Chem. Eng. Sci.* **1996**, *51*, 1121 – 1132.

(20) Larfeldt, J.; Leckner, B.; Melaaen, M. C. *Fuel* **2000**, *79*, 1637–1643.

(21) Grønli, M. G. A theoretical and experimental study of the thermal degradation of biomass. PhD thesis, Norwegian University of Science and Technology, Trondheim, Norway, 1996.

(22) de Paiva Souza, M. E.; Nebra, S. A. *Wood Fiber Sci.* **2000**, *32*, 153–163.

(23) Evans, D.; Emmons, H. *Fire Saf. J.* **1977**, *1*, 57 – 66.

(24) Wornat, M. J.; Hurt, R. H.; Davis, K. A.; Yang, N. Y. *Symp. (Int.) Combust.* **1996**, *26*, 3075 – 3083.

(25) Branca, C.; Di Blasi, C. *Energy Fuels* **2003**, *17*, 1609–1615.

(26) National Laboratory Lawrence Livermore, SUNDIALS: SUite of Nonlinear and DIfferential/ALgebraic Equation Solvers - IDA. 2016; http://computation.llnl.gov/projects/sundials/ida [accessed 2017-04-07].

(27) Hermansson, S.; Thunman, H. *Combust. Flame* **2011**, *158*, 988 – 999.

This is the accepted version of an article published in Energy and Fuels
DOI: 10.1021/acs.energyfuels.8b00777

(28) Bird, R. B.; Stewart, W. E.; Lightfoot, E. N. *Transport Phenomena*, 2nd ed.; John Wiley & Sons, Inc.: New York, 2002.

(29) Forest Products Laboratory, *Wood Handbook - Wood as an Engineering Material. General Technical Report FPL–GTR–190*; 2010.

(30) Biswas, A. K.; Umeki, K. *Chem. Eng. J.* **2015**, *274*, 181 – 191.

(31) Hagge, M. J.; Bryden, K. M. *Chem. Eng. Sci.* **2002**, *57*, 2811 – 2823.

(32) Wagenaar, B.; Prins, W.; van Swaaij, W. *Fuel Process. Technol.* **1993**, *36*, 291 – 298.

(33) Chan, W.-C. R.; Kelbon, M.; Krieger, B. B. *Fuel* **1985**, *64*, 1505–1513.

(34) Liden, A.; Berruti, F.; Scott, D. *Chem. Eng. Commun.* **1988**, *65*, 207–221.

(35) Koufopanos, C.; Papayannakos, N.; Maschio, G.; Lucchesi, A. *Can. J. Chem. Eng.* **1991**, *69*, 907–915.

(36) Di Blasi, C. *Combust. Sci. Technol.* **1993**, *90*, 315–340.

(37) Bryden, K. M.; Hagge, M. J. *Fuel* **2003**, *82*, 1633 – 1644.

(38) Neves, D.; Thunman, H.; Matos, A.; Tarelho, L.; Gomez-Barea, A. *Prog. Energy Combust. Sci.* **2011**, *37*, 611 – 630.

(39) Fatehi, H. Numerical Simulation of Combustion and Gasification of Biomass Particles. PhD thesis, LTH (Lund University), Lund, Sweden, 2014.

(40) Jones, J.; Bridgeman, T.; Darvell, L.; Gudka, B.; Saddawi, A.; Williams, A. *Fuel Process. Technol.* **2012**, *101*, 1 – 9.

(41) Fisher, E.; Dupont, C.; Darvell, L.; Commandré, J.-M.; Saddawi, A.; Jones, J.; Grateau, M.; Nocquet, T.; Salvador, S. *Bioresour. Technol.* **2012**, *119*, 157 – 165.

This is the accepted version of an article published in Energy and Fuels
DOI: 10.1021/acs.energyfuels.8b00777

(42) McNamee, P.; Darvell, L.; Jones, J.; Williams, A. *Biomass Bioenergy* **2015**, *82*, 63 – 72.

This is the accepted version of an article published in Energy and Fuels
DOI: 10.1021/acs.energyfuels.8b00777